Journal of Controlled Release 390 (2026) 114538

Contents lists available at ScienceDirect

Journal of Controlled Release

journal homepage: www.elsevier.com/locate/jconrel

Biodynamers as prodrugs with controlled uptake and activity☆

Thi Thu Nguyen [a], Jan Hemmer [b], Alexandra K. Kiemer [b], Britta Diesel [b], Sangeun Lee [a,c,*]

[a] Saarland University, Department of Pharmacy, Pharmaceutical Materials and Processing, PharmaScienceHub (PSH), Saarbrücken, Germany
[b] Saarland University, Department of Pharmacy, Pharmaceutical Biology, PharmaScienceHub (PSH), Center for Gender-Specific Biology and Medicine (CGBM), Saarbrücken, Germany
[c] Helmholtz Institute for Pharmaceutical Research Saarland (HIPS), Helmholtz Centre for Infection Research (HZI), Saarbrücken, Germany

ARTICLE INFO

Keywords:
pH-responsive polymeric prodrug
Adenosine dialdehyde
Anticancer
Spheroids
Tumor microenvironment
Biodynamers

ABSTRACT

Chemotherapy is one of the primary approaches for cancer treatment. However, its toxicity to healthy tissue often causes significant side effects, which is one of the main reasons why many potent drug candidates fail to gain therapeutic approval. Adenosine dialdehyde (ADOX), an adenosine analog used as an indirect methylation inhibitor that hinders S-adenosyl homocysteine hydrolase (SAHH), is one such promising candidate affected by this limitation. In this study, we developed a polymeric prodrug of ADOX to reduce its toxicity to non-cancerous cells under neutral conditions and to enhance its selectivity toward cancer cells in the acidic tumor microenvironment (TME). Specifically, we designed ADOX-biodynamers, alternative copolymers based on dynamic constitutional chemistry, that release ADOX from their backbone in response to the acidic pH of the TME. The ADOX-biodynamers were prepared by connecting two monomers, ADOX and amino acid hydrazides (Lys-Hz, His-Hz, Phe-Hz, and Glu-Hz), alternatively *via* pH-responsive dynamic covalent bonds, imines, and acylhydrazones. The dynamic covalent bonds allow degradation of ADOX-biodynamers, enabling the release of ADOX under acidic conditions. In particular, ADOX-Lys biodynamer (ALB) released ADOX under acidic conditions at a rate 8 times faster than in neutral conditions. In contrast, at pH 7.4, ALB maintained a stable polymeric structure, which suppressed ADOX activity and reduced toxicity up to 5 times compared to the free ADOX in non-cancerous cells, 16HBE14o-. However, when ALB was first exposed to acidic conditions, it regained its cytotoxicity toward three human cancer cell lines: HCT116, MCF-7, and SW480, recovering up to 60 % of the activity of free ADOX. In addition, ALB exhibited significantly higher cellular uptake under mildly acidic conditions (pH 6.4), with nearly twice the uptake compared to that at pH 7.4. Notably, in an *in vitro* tumor tissue model using HCT116 spheroids, ALB treatment resulted in a substantial reduction in spheroid size, achieving approximately a 40 % decrease after 7 days of treatment. As a result, the synthesized ADOX-biodynamers demonstrated improved safety toward non-cancerous cells in neutral pH, restored the activity of the free drug and increased cellular uptake in acidic conditions, and effectively penetrated into tumor tissue. These findings indicate that ADOX-biodynamers successfully address the limitations of ADOX and serve as an effective delivery system. This study highlights the potential of polymeric prodrugs utilizing dynamic covalent bonds as a promising strategy to simultaneously improve drug safety and therapeutic efficacy, supporting the development of potent therapeutic candidates.

1. Introduction

Chemotherapeutic agents, such as doxorubicin, paclitaxel, and gemcitabine, have played a crucial role in cancer treatment and have remained the first-line choice for advanced-stage malignancies of various cancers where surgery or radiation therapy is not feasible [1]. However, their adverse side effects, *i.e.*, toxicity and non-selectivity, have remained the main drawbacks [2–4]. High systemic toxicity, off-

Abbreviations: ADOX, Adenosine dialdehyde; SAHH, S-adenosyl homocysteine hydrolase; TME, Tumor microenvironment; ALB, ADOX-Lysine biodynamer; AHB, ADOX-Histidine biodynamer; APB, ADOX-Phenylalanine biodynamer; AGB, ADOX-Glutamate biodynamer; Rho-ALB, Rhodamine-labeled ADOX-Lysine biodynamer; Con-A, Concanavalin Alexa 488; MoA, Mechanism of action; CLSM, Confocal Laser Scanning Microscope.

☆ This article is part of a Special issue entitled: 'Young Investigator Issue' published in Journal of Controlled Release.

* Corresponding author at: Saarland University, Department of Pharmacy, Pharmaceutical Materials and Processing, PharmaScienceHub (PSH), Saarbrücken, Germany.
E-mail address: Sangeun.Lee@uni-saarland.de (S. Lee).

https://doi.org/10.1016/j.jconrel.2025.114538
Received 30 April 2025; Received in revised form 19 August 2025; Accepted 11 December 2025
Available online 14 December 2025

target effects, or instability are also significant limitations in the clinical application of many potent candidates, such as camptothecins, thapsigargin, and adenosine dialdehyde (ADOX) [5–7]. Efforts to reduce the toxicity and enhance the selectivity and pharmacokinetics of such potent candidates through innovative delivery systems or structural modifications are a key focus in the recent development of new anticancer drugs. The advances in targeted delivery mitigate these limitations, resulting in the clinical approval or move toward clinical trials of their derivatives. For instance, irinotecan, a clinically approved prodrug of camptothecin, overcame the parent compound's instability and toxicity, or mipsagargin, a prostate-specific antigen-activated prodrug of thapsigargin, has progressed to Phase I/II clinical trials [8,9]. Similarly, ADOX, a compound recognized for its highly potent anticancer activity for over 40 years, remains excluded from clinical evaluation due to its toxicity and non-selectivity, highlighting the continued need for innovative delivery approaches [10]. ADOX is an adenosine analog with substantial potential in cancer therapy and has long been utilized as a pharmacological tool to explore the role of methylation in cellular processes and study epigenetics [5]. ADOX acts as an inhibitor of S-adenosylhomocysteine hydrolase (SAHH), an enzyme that regulates cellular methylation processes, resulting in broad inhibition of methylation reactions, including those of DNA, RNA, and proteins [11–14]. Over the years, ADOX has demonstrated anticancer effects in various *in vitro* and *in vivo* models, such as in prostate cancer [15], embryonic carcinoma [16], breast cancer [17], and colon adenocarcinoma [18]. Additionally, ADOX was proven to effectively arrest the cell cycle at the G2 phase and induce p53-dependent apoptosis in HeLa, HCT116, and Human T-lymphotropic virus type 1 cells (HTLV-1) [18–20]. In particular, ADOX also inhibits isoprenylcysteine carboxyl methyltransferase (ICMT), leading to decreased MMP-9 levels and thereby mitigating the migratory and invasive capabilities of breast cancer and glioma cells [16]. Consequently, ADOX is a potent candidate for further development as an anticancer drug for preventing or curing various cancers with broad inhibiting proliferative effects and anti-invasive and anti-migratory properties through clearly proven mechanisms [17].

However, one of the biggest challenges to further developing ADOX is its toxicity and lack of selectivity, which leads to off-target effects. ADOX could disrupt the methylation processes and nucleotide metabolism in the whole body because of the presence of SAHH enzymes in both healthy and cancer cells, potentially leading to severe toxicity [21]. Another concern regarding the toxicity of ADOX is related to the interaction of its aldehyde groups with proteins through crosslinking reactions, further hindering its clinical application [10,22]. Therefore, several strategies have been demonstrated to overcome ADOX's limitations, aiming to mitigate its toxic effects by reducing its impact on normal cells while enhancing its selectivity for cancer cells [22,23]. Previous efforts to reduce ADOX's toxicity have involved modifying ADOX into a nucleoside monoaldehyde. Reducing the amount of aldehyde groups could decrease the crosslinking reactions, minimizing the interactions of ADOX with proteins [22]. However, even with this modification, ADOX continues to exhibit its toxicity to normal tissue due to the broad impact of methylation. Therefore, it remains essential to continuously explore alternative approaches to address the limitations of this drug.

Implementing smart drug delivery systems to deliver therapeutic agents selectively toward tumor sites is an important aspect of drug development [24]. Smart drug delivery systems are designed to respond to environmental factors, such as pH, temperature, light, reduction/oxidation, and enzymes, causing a dramatic change in their physicochemical properties and releasing the drug [25]. This capability can also enhance controlled release and activity of drugs at the tumor sites based on the response of the TME. Compared to normal tissue, the TME possesses several distinct characteristics, including an acidic pH, hypoxia, and elevated levels of specific enzymes [26]. These features have been utilized to develop such smart drug delivery systems, using stimulus-responsive polymers [27–30]. Among these, pH-responsive polymers are commonly used, as a decrease in pH is frequently observed in most solid tumors [31]. Typically, the extracellular pH in the TME is usually more acidic, ranging from pH 6.5 to 6.9, while the physiological pH of healthy tissue lies between 7.2 and 7.5 [32]. This acidic environment is a result of the increased glycolytic activity in cancer cells, which converts glucose into lactic acid to produce the energy required for their survival [33].

Biodynamers, proteinoid dynamic biopolymers composed of amino acid hydrazide and dialdehyde monomers, have emerged as promising carriers in pH-responsive drug delivery systems due to their adaptive properties, enabled by dynamic covalent bonds [34]. These biodynamers were polymerized through acylhydrazone and imine bonds, both of which are responsive to weak acidity [35,36]. Particularly, biodynamers possess similar structural and functional characteristics to natural biopolymers, such as peptides and proteins. This resemblance confers several advantages for biodynamer when used as a drug carrier, including enhanced biocompatibility, biodegradability, and functionality [37]. Accordingly, the biodynamers were demonstrated as novel pharmaceutical materials in nucleotide and protein delivery [38,39], drug potentiators [40], and the ionic sensing agent [41], featuring pH-responsive dynamic covalent bonds. For instance, Dynaplexes, the protein-based biodynamers featuring pH-sensitive linkers, exhibit significant promise as vectors for siRNA transfection. Their excellent biocompatibility, ease of tunability, and ability to undergo dynamic polymerization in acidic environments contribute to their effectiveness. Using Dynaplexes for the delivery of siRNA enables a robust knockdown of survivin mRNA, leading to a pronounced induction of apoptosis in carcinoma cells and demonstrating efficacy that is 2.2 times greater than that observed with the lipid-based transfection agent [38]. Another example is about Arg-biodynamers, which demonstrate 32-fold greater effectiveness against *E. coli* than colistin and are over 128-fold less toxic to mammalian cells than poly-L-arginine, while maintaining similar antibacterial activity. Their dynamicity, biodegradability, and biocompatibility make Arg-biodynamers promising adjuvants in the fight against Gram-negative bacteria and antimicrobial resistance [40]. Furthermore, cationic lysine-based biodynamers display pH-dependent morphological and optical properties, emphasizing their significant potential for targeted drug delivery, especially to tumor sites [37].

In this study, we leveraged the chemical structure of ADOX to develop ADOX-biodynamers through the polymerization of the active site of ADOX (aldehydes) with amino acid hydrazides of different side chains, Lys, His, Phe, and Glu (Scheme 1). With the pH-responsive dynamic covalent bonds, acylhydrazones, and imines in the ADOX-biodynamers, these polymers enable the release of ADOX and reveal its active site through degradation when exposed to low pH at the tumor site. This targeted release mechanism allows the controlled activation of ADOX specifically at the tumor site while keeping it inactive in normal tissues through its polymeric prodrug form. Here, we prove the concept of a pH-responsive polymeric ADOX-prodrug with dynamic covalent bonds as a strategy for overcoming the conventional limitations of selectivity and safety.

2. Materials and methods

2.1. Materials and instruments

ADOX was purchased from Sigma-Adrich (USA, #SLCB1334), L-Lysine methylester 2HCl, L-Histidine methylester 2HCl, L-Phenylalanine methylester HCl, L-Glutamic acid -1 methylester Hydrazine hydrate, NHS-Rhodamine (5/6-carboxy-tetramethyl-rhodamine succinimidyl ester), and Concanavalin Alexa 488 were purchased from Thermo Fisher Scientific (Germany). Invitrogen Hoechst 33342 was purchased from Lumiprobe (USA). Dimethyl sulfoxide (DMSO) and acetonitrile (HPLC grade) were purchased from Fisher Scientific (Schwerte, Germany). Lactate Dehydrogenase (LDH) Colorimetric Assay Kit was purchased from Invitrogen (Thermo Fisher, USA), Dulbecco's Modified Eagle's

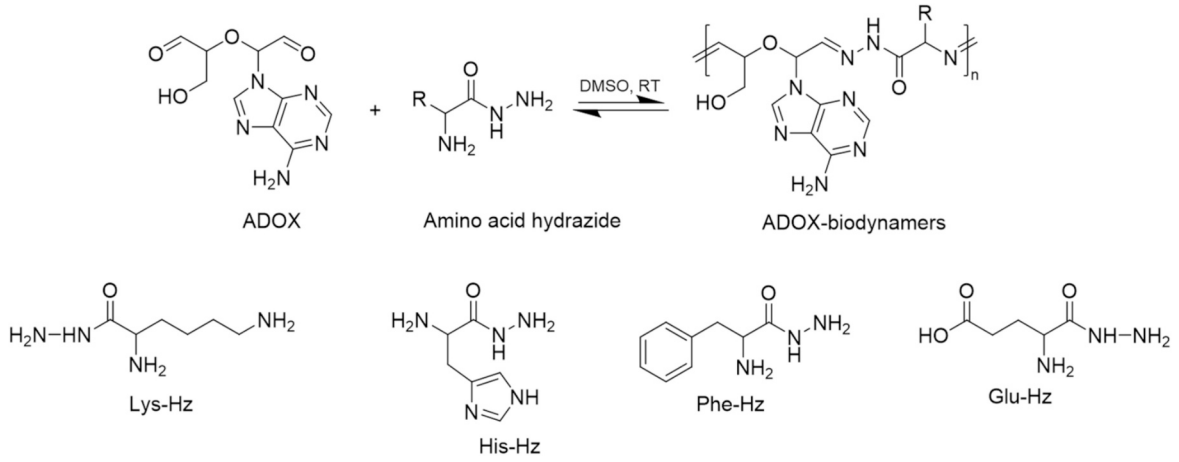

Scheme 1. Synthesis of ADOX-biodynamers from different amino acid hydrazides side chains (R = side chain of Lys, His, Phe and Glu).

Medium (DMEM), Hanks' Balanced Salt Solution (HBSS), RPMI 1640 medium, methylthiazol tetrazolium (MTT), 4′, 6-diamidino-2-phenylindole (DAPI), and paraformaldehyde were purchased from Sigma-Aldrich (Darmstadt, Germany), M199 medium was purchased from PAN Biotech (Germany), Apoptosis/Necrosis Detection Kit (blue, green, red, ab176749) was purchased from Abcam. Unless otherwise specified, all reagents were purchased from Sigma-Aldrich. ^{1}HNMR spectra were recorded on a Bruker AVANCE 500 (500 MHz) spectrometer at 300 K, using pulse accumulation of 64 scans and the LB parameter of 0.30 Hz. HPLC was performed on a Dionex UltiMate 3000 series system (Thermo Fisher, Dreieich, Germany).

All commercially available reagents were used without any further purification.

2.2. Cell culture

Cell lines were from ATCC. SW480 human colorectal adenocarcinoma cells were cultured in RPMI 1640 medium (Sigma-Aldrich, #R8758), MCF-7 human breast cancer cells, and HCT116 human colorectal cancer cells were cultured in DMEM (Sigma-Aldrich, #D6546). Mediums were supplemented with 10 % fetal calf serum (FCS) (Pan-Biotech, #P040–37500), 2 mM glutamine (Sigma-Aldrich, #G7513), 100 U/mL penicillin, and 100 μg/mL streptomycin (Sigma-Aldrich, #P4333). Cells were cultured at 37 °C in a humidified atmosphere of 5 % CO_2. Subculturing was performed according to the ATCC recommendations.

16HBE14o- human bronchial epithelial cells, provided by Dr. Gruenert (University of California, San Francisco, USA), were cultured as previously described [42]. Firstly, fibronectin coating solution was prepared by mixing human fibronectin (1 mg/mL, Sigma F114), collagen (3 mg/mL in 0.2 % sterile acetic acid, Roche 1,179,179), and bovine serum albumin (1 mg/mL, 0.1 % solution, UCSF code NEBZR285) in LHC basal medium (Invitrogen, 12677–019). Before seeding cells, all tissue culture plasticware was coated with the fibronectin coating solution. 16HBE14o- cells were then cultured in M199 medium (PAN Biotech) supplemented with 10 % fetal calf serum (PAN Biotech, #P040–37500), 2 mM glutamine (Sigma-Aldrich, #G7513), 100 U/mL penicillin, and 100 μg/mL streptomycin (Sigma-Aldrich, #P4333). The cells were maintained at 37 °C in a humidified atmosphere containing 5 % CO_2 and subcultured following the same protocol used for other cell lines.

2.3. Synthesis of amino acid hydrazides

Lysine-hydrazide (Lys-Hz). To a solution of L-Lysine methyl ester 2HCl (100 mg, 0.62 mmol) in methanol (2 mL), hydrazine monohydrate (160 mg, 4.96 mmol) was added. The reaction mixture was stirred at room temperature for 24 h, and then MeOH was removed using a rotary evaporator. The residue was dissolved in H_2O and lyophilized. Phe-Hz, Glu-Hz, and His-Hz were prepared from L-Phenylalanine methyl ester HCl, L-Glutamic acid -1 methyl ester, and L-Histidine methyl ester 2HCl, respectively, using the same protocol as Lys-Hz. The freeze-dried compounds were then analyzed by NMR spectroscopy (^{1}HNMR, D_2O, Fig. S1 and Table S1).

2.4. Synthesis and characterization of ADOX-biodynamers

ADOX was mixed with Lys-Hz, His-Hz, Phe-Hz, or Glu-Hz in DMSO in an equal molar ratio (100 mM) and stirred at room temperature (exclusion of light) to synthesize ADOX-Lysine biodynamer (ALB), ADOX-Histidine biodynamer (AHB), ADOX-Phenylalanine biodynamer (APB), and ADOX-Glutamate biodynamer (AGB). Then, the products were washed by dialysis (Dialysis membrane tubing spectra/Por® 7, 3.5 kDa) against DMSO for 24 h to remove free monomers. The purified polymers were precipitated in MeOH to remove DMSO and dried under vacuum. The synthesized polymers were monitored and characterized using NMR spectroscopy, UV-VIS spectrometry, and light scattering.

2.4.1. NMR spectroscopy

The polymerization was conducted in DMSO-d_6 and monitored using ^{1}HNMR at specific time points. The measurements were performed at 0, 1, and 42 h for ALB, 0,1, and 48 h for APB and AGB, 0 and 24 h for AHB.

2.4.2. UV-VIS spectrometry

The mixtures of the ADOX and amino acid hydrazide (Lys-Hz, His-Hz, Phe-Hz, and Glu-Hz) were prepared in DMSO with a final concentration of 100 mM. At each time point (1, 2, 4, 6, 24, 30, 42, and 48 h), 2 μL of the reaction solution was diluted with 198 μL of DMSO. The solutions were placed in a 96-well plate, and their absorbance (260–450 nm) was measured using a Tecan Reader® Infinite M200 microplate spectrophotometer (Tecan, Männedorf, Switzerland). The change in absorption wavelength during the synthesis process was meticulously recorded at each time point for all synthesized biodynamers (ALB, AHB, APB, and AGB).

2.4.3. Static light scattering (SLS)

Static light scattering (SLS) was employed to assess the molecular weight of the ALB using Zetasizer Ultra (Malvern Panalytical, Malvern, UK). A range of concentrations of ALB in DMSO was prepared (10, 7.5, 5, 2.5, and 1 mM) and placed in a quartz cuvette for measurement. The scattered intensity averaged was measured over a period of 10 to 30 s for different analyte concentrations and for the DMSO as solvent alone.

Using static Debye plot analysis, a linear regression fit allows determining the intercept and the slope of the straight line from which M_w is deduced. The experiment was analyzed in triplicate ($n = 3$).

2.5. pH-dependent ADOX release from ADOX-biodynamers

The release of ADOX from ADOX-biodynamers at various pH levels was conducted using the dialysis method. ALB or AHB (10 mM/mL) was placed in a dialysis membrane (MWCO 1 kDa) and put in 10 mM acetate buffer (pH 5.4), MES buffer (pH 6.4), and phosphate buffer (pH 7.4) at 37 °C. At each time point (1, 2, 4, 24, 48, and 96 h) the solution of ALB outside the membranes was taken out and analyzed by HPLC (Mobile phase, 7 % ACN; Flow rate, 0.8 mL/min; Detection at 284 nm *via* UV-VIS detector, C18 column, 250 $\underline{\times}$ 4.6 mm with 5 μm particle size. For AHB, the mobile phase was adjusted to 10 % ACN and 0.01 M CH_3COONH_4, pH 5.4. The amount of the released ADOX was compared using a calibration curve prepared from the free ADOX in buffers of different pH, with each analytical run performed in triplicate under the same HPLC measurement conditions.

Note that, due to APB's precipitation in the eluent, making analysis difficult, it was excluded from further experiments.

2.6. MTT assay

The antiproliferative effects of ADOX and ALB at neutral conditions were assessed using the MTT assay on the cancer cell lines HCT116, MCF-7, SW480, and non-cancerous 16HBE14o- cells. Cells were seeded in 96-well plates 24 h before treatment, at a density of 1.5×10^5 cells/mL for HCT116 and MCF-7, 10^5 cells/mL for SW480, and 8×10^4 cells/mL for 16HBE14o-. Cells were treated with ADOX and ALB at concentrations of 25, 50, 100, 200, and 400 μM. Stock solutions of ADOX and ALB (100 mM) were prepared in DMSO and diluted with medium to ensure a final DMSO concentration of 0.4 % in all treatment groups. Accordingly, cells treated with 0.4 % DMSO alone were used as the negative control. Following an incubation period of 72 h, the cells were incubated with MTT solution (0.5 mg/mL) for 30 min for HCT116, 90 min for MCF-7, 120 min for SW480, and 75 min for 16HBE14o-. Cell viability was evaluated by measuring the absorbance at 560 nm using a microplate reader (GloMax™, Promega, Germany), according to the following equation:

$$\%\ Cell\ viability = \frac{A_{560} treated\ cell \times 100}{A_{560} untreated\ cell}$$

To evaluate the effect of activated ALB on cell viability, we conducted MTT assays on HCT116, MCF-7, SW480, and 16HBE14o- cell lines after the pre-activation of ALB under acidic conditions. ALB was pre-incubated in 10 mM acetate buffer at pH 5.4 for 48 h to facilitate its degradation and activation of ADOX. The samples were then lyophilized and dissolved again in DMSO. The solution was diluted with each medium (*details in 2.2. Cell culture*) and subsequently treated with each cell line at various concentrations (25, 50, 100, 200, and 400 μM). After a 72-h incubation with the cells, the MTT assay was performed to evaluate the effect of pre-activated ALB as described above.

The assays were performed in triplicate ($N = 3$, $n = 5$). IC_{50} values were calculated by non-linear regression using GraphPad Prism.

2.7. LDH (lactate dehydrogenase) assay

Membrane integrity was measured using the Lactate Dehydrogenase (LDH) Colorimetric Assay Kit (Invitrogen, Thermo Fisher). HCT116 cells (1.5×10^5/mL) were seeded into a 96-well plate 24 h prior to treatment. Then, the cells were treated with varying concentrations of ADOX and ALB. Cells cultured in a medium containing 0.4 % DMSO served as the control. After 72 h of incubation, 50 μL of the medium was transferred to a separate plate. Then, 50 μL of the Reaction Mixture was added, mixed well with the samples, and the plate was incubated at room temperature for 30 min, protected from light. After that, 50 μL of Stop Solution was added to each sample well, and the absorption was measured at 490 nm and 680 nm by a microplate reader (GloMax™, Promega, Germany). The cytotoxicity of samples was calculated using the following formula.

$$\%\ Cytotoxicity = \left[\frac{Compound\ treated\ LDH\ activity - Spontaneous\ LDH\ activity}{Maximum\ LDH\ activity - Spontaneous\ LDH\ activity}\right] \times 100$$

2.8. Apoptosis/necrosis dye staining

To determine the mode of cell death, either apoptosis or necrosis, cells were stained with the Apoptosis/Necrosis Detection Kit (blue, green, red, ab176749, Abcam) following the protocol provided by Abcam and analyzed with CLSM. Briefly, HCT116 cells were seeded at a density of 5×10^4 cells/well in a μ-Slide 8-Well (Ibidi) and incubated for 24 h to allow attachment. The cells were then treated with either ADOX or ALB (100 μM) for 24 h. Following the treatment, the cells were washed twice with the assay buffer provided in the kit and incubated with the staining solution for 45 min at room temperature in the dark. After the incubation, the cells were washed twice with 200 μL of assay buffer and then replaced with fresh assay buffer for analysis. Using CLSM, apoptotic cells, identified by the binding of Apopxin Green Indicator to phosphatidylserine (PS), were visualized using the FITC channel (Ex/Em = 490/525 nm). Necrotic cells were identified by 7-AAD uptake, showing red fluorescence on the Texas Red channel (Ex/Em = 550/650 nm). Healthy cells were detected by CytoCalcein Violet 450, displaying blue fluorescence in the DAPI channel (Ex/Em = 405/450 nm).

2.9. Cellular uptake analysis

To analyze the uptake of ALB, the ALB was first labeled with Rhodamine-NHS. The ALB was mixed with Rhodamine-NHS in DMSO at a 10:1 ratio to achieve 10 % dye conjugation on the polymer side chains. The unbound dye was removed by dialysis against DMSO for 24 h. The resulting Rhodamine-labeled ADOX-Lysine biodynamer (Rho-ALB) was then lyophilized and re-dissolved in DMSO. The cell uptake of Rho-ALB was analyzed by Flow cytometry and CLSM.

2.9.1. Flow cytometry

HCT116 cells (2×10^5 cells/well) were seeded into six-well plates and incubated for 48 h before treatment. Rho-ALB dissolved in DMSO was diluted with HBSS (60 μg/mL), adjusted to pH 7.4 or 6.4, and incubated with the cells for 2 h. After the incubation, the cells were washed twice with PBS, and a single-cell suspension was prepared by trypsinization. The cells were harvested and centrifuged at 300 ×*g* for 5 min at 4 °C. They were then fixed with 1 % paraformaldehyde (PFA) and incubated in the dark for 20 min. After removing the fixing solution by another round of centrifugation (300 ×*g*, 5 min, 4 °C), the cells were resuspended in PBS. Flow cytometry was performed on a BD LSR

Fortessa, and a total of 10,000 events were acquired. The data were processed with BD FACS Diva software (BD Biosciences), and the median fluorescence intensity of the singlet cells was used to quantify ALB uptake in HCT116 cells.

2.9.2. CLSM

HCT116 cells (2×10^5 cells/mL) were seeded in a μ-Slide 8-Well (Ibidi) and incubated for 24 h before treatment. The cells were then incubated with Rho-ALB (60 μg/mL) in HBSS adjusted to pH 7.4 or 6.4 for 2 h. After incubation, the cells were washed twice with PBS and stained with DAPI and Concanavalin Alexa 488 (Con-A). The cells were visualized using CLSM (LSM 710, Carl Zeiss AG, Jena, Germany) with an EC Plan-Neofluar 63× water immersion objective. Signals from all channels (DAPI at Ex/Em = 358/461 nm, Con-A at Ex/Em = 495/519 nm, and Rhodamine at Ex/Em = 552/575 nm) were acquired and merged. The images were processed using Fiji software.

2.10. ADOX-biodynamer efficacy on tumor spheroids

2.10.1. Spheroid formation

HCT116 cells (5×10^4 cells/mL) were seeded into a 96-well clear, round-bottom, ultra-low attachment plate (MS-9096UZ, Sbio, Akita Sumitomo Bakelite, Japan). The plates were then centrifuged at 300 ×*g* for 5 min to facilitate cell aggregation, followed by incubation for 72 h at 37 °C in a humidified 5 % CO_2 atmosphere to form spheroids.

2.10.2. Anti-proliferation effect of ALB on spheroids

Prepared HCT116 spheroids were treated with ADOX or ALB at concentrations of 50, 100, 200, and 400 μM for 7 days. After the incubation, the area of spheroids was measured by microscopy (IncuCyte S3, Sartorius). The relative spheroid area was used to evaluate the anti-proliferation effect of ADOX and ALB on HCT116 cells. The relative spheroid area was measured using the following formula.

$$\textit{Relative spheroid area} = \frac{\textit{Spheroid area}\ (T_t)}{\textit{Spheroid area}\ (T_0)}$$

T_0: Spheroid area (μm^2) measured from the spheroid after 3 days of culture.

T_t: Spheroid area (μm^2) measured after t days of treatment with ALB or ADOX.

2.10.3. ALB penetration into spheroids

To evaluate the penetration of ALB in spheroids, Rho-ALB (60 μg/mL) was incubated with prepared HCT116 spheroids for 24 h. Following incubation, spheroids were stained with Hoechst 33342 (10 μg/mL) (Lumiprobe, Germany) for 45 min. After washing with HBSS, samples were visualized by CLSM (LSM 710, Carl Zeiss AG, Jena, Germany) with Ex/Em = 350/461 nm for Hoechst, Ex/Em = 552/575 nm for Rho-ALB. *Z*-stack images were acquired at 30 μm intervals to a total depth of approximately 540 μm, using a 10× objective. The z-stack images were processed using Fiji software to calculate the mean fluorescent intensity.

2.11. Statistical analysis

The results are presented as mean values ± standard deviation from at least three independent experiments. One-way analysis of variance (ANOVA) and Student's *t*-tests (t-test) were performed to determine the statistical significance between the groups at $p > 0.05$ (no statistical difference, ns), $^*p < 0.05$, $^{**}p < 0.01$, $^{***}p < 0.005$, and $^{****}p < 0.0001$. Statistical analysis was conducted using GraphPad Prism software (version 8.0.2, 2019) and Microsoft Excel software (2021).

3. Results and discussion

3.1. Synthesis of ADOX-biodynamers

Biodynamers can be polymerized using various amino acid derivatives, and the side chains of the amino acid influence biodynamers'

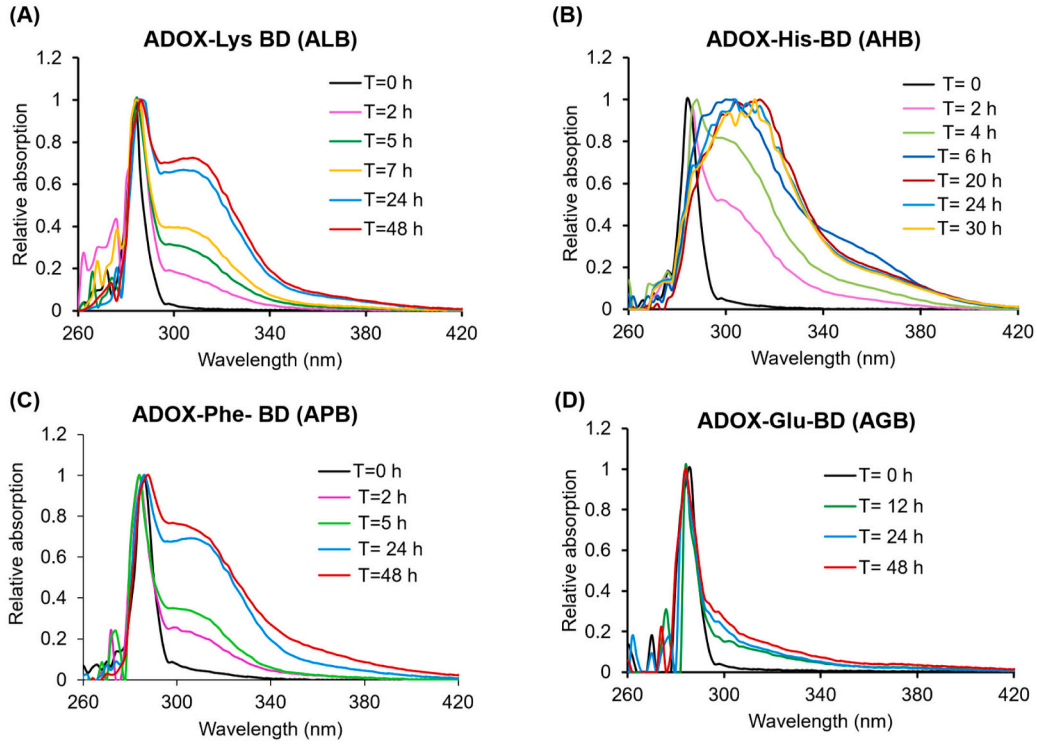

Fig. 1. Absorption changes as a function of reaction time in the synthesis process of (A) ALB, (B) AHB, (C) APB and (D) AGB.

physicochemical properties, such as polymerization degree, degradation rate, and cellular uptake. Therefore, to compare the effects of side chains, we prepared hydrazide (Hz) derivatives of Lys, His, Phe, and Glu, as well as four types of ADOX-biodynamers using each amino acid-Hz. ADOX and each amino acid hydrazide (Lys-Hz, His-Hz, Phe-Hz, or Glu-Hz, synthesized similarly following the previously reported method [39] were reacted at an equal molar concentration in DMSO. The reactions between the monomers were monitored and characterized using UV-VIS spectrometry, ^{1}HNMR, HPLC, and SLS.

ADOX reacted with Lys-Hz, His-Hz, and Phe-Hz, exhibiting a colour change from colorless to yellow. Notably, there was an increase in absorbance in the 310–330 nm region (Fig. 1A–C), which is known to be associated with imine and acylhydrazone bonds [43,44]. Therefore, the absorption changes of the mixtures of ADOX and Lys-Hz, His-Hz, or Phe-Hz support their reaction and the successful formation of acid-responsive dynamic covalent bonds. The absorption increases reached saturation after 42 h for Lys-Hz, 24 h for His-Hz, and 48 h for Phe-Hz, indicating the completion of the reaction.

However, no such change was observed in the mixture of ADOX and Glu-Hz, suggesting the formation of relevant dynamic covalent bonds was inefficient among the monomers (Fig. 1D). This may be due to the negative charge of Glu-Hz, which is known to hinder the reaction and polymerization of biodynamers [45]. It was also observed in previously reported proteoid biodynamers, composed of amino acid-Hz and hexamethylene glycol-conjugated carbazole dialdehyde. These biodynamers, with positively charged monomers such as Lys-Hz and His-Hz, exhibited higher M_w due to efficient polymerization facilitated by attractive charge interactions with the electron clouds on the carbazoles. In contrast, polymerization with the negatively charged Glu-Hz yielded lower M_w because of the repulsions between the negative charges of the Glu-Hz and π-electrons of the carbazoles [45]. Thus, a similar phenomenon occurred in the reaction between ADOX and Glu-Hz, rendering their reaction ineffective under the experimental conditions.

The formation of dynamic covalent bonds was further confirmed using ^{1}HNMR. Fig. 2A shows the ^{1}HNMR spectra of ADOX and Lys-Hz mixture after 1 and 42 h, and free ADOX. After 42 h, the proton peak of the aldehydes (δ 9.5 ppm) was completely flattened. It represents the completion of the reaction by the consumption of aldehydes on ADOX. In addition, the gradual broadening of signals for aromatic protons, observed between δ 7.8 and 8.6 ppm, indicates the presence of repeating aromatic units, further confirming successful polymerization. This phenomenon has also been reported in the imine and acyl hydrazone-based polymeric structures [46]. A similar change was observed in the ^{1}HNMR spectra during the synthesis of AHB and APB, except for AGB (see Fig. S2, S3, and S4). In the AGB case, the broadening of the peaks corresponding to imines and acylhydrazones was not observed.

Note that the ^{1}HNMR spectra of nucleoside dialdehydes, such as ADOX, are known to be extremely complex. They consist of several isomers in dynamic equilibrium, resulting in the complicated analysis of the ^{1}HNMR spectrum [22]. This complexity explains the numerous peaks observed in the spectra of free ADOX.

After the reaction, ADOX-biodynamers were purified by dialysis against DMSO to remove unreacted monomers and oligomers, smaller than 3.5 kDa. The resulting polymers were collected and analyzed *via* HPLC to compare their retention times (Rt) with free ADOX. The Rt of ALB (Fig. 2B, Rt = 4.91 ± 0.23) and AHB (Fig. 2C, Rt = 3.15 ± 0.18) increased after washing compared to free ADOX (Rt = 2.39 ± 0.15 and 1.83 ± 0.12). The increase in Rt is also a signal of polymerization, as an increase in M_w can result in reduced solubility and increased interaction with the column under the applied measurement conditions (see the Methods). In the case of APB, its solubility decreased significantly, and restricted HPLC analysis. Therefore, APB was excluded from further investigation.

Additionally, GPC was first used to analyze the M_w of the washed ADOX-biodynamers. However, the limited solubility of ADOX-biodynamers made GPC analysis difficult for accurate M_w determination. Complementary, SLS was employed to estimate the M_w of ALB. The SLS data indicated that the average M_w of ALB is 49 ± 29 kDa (Fig. S5).

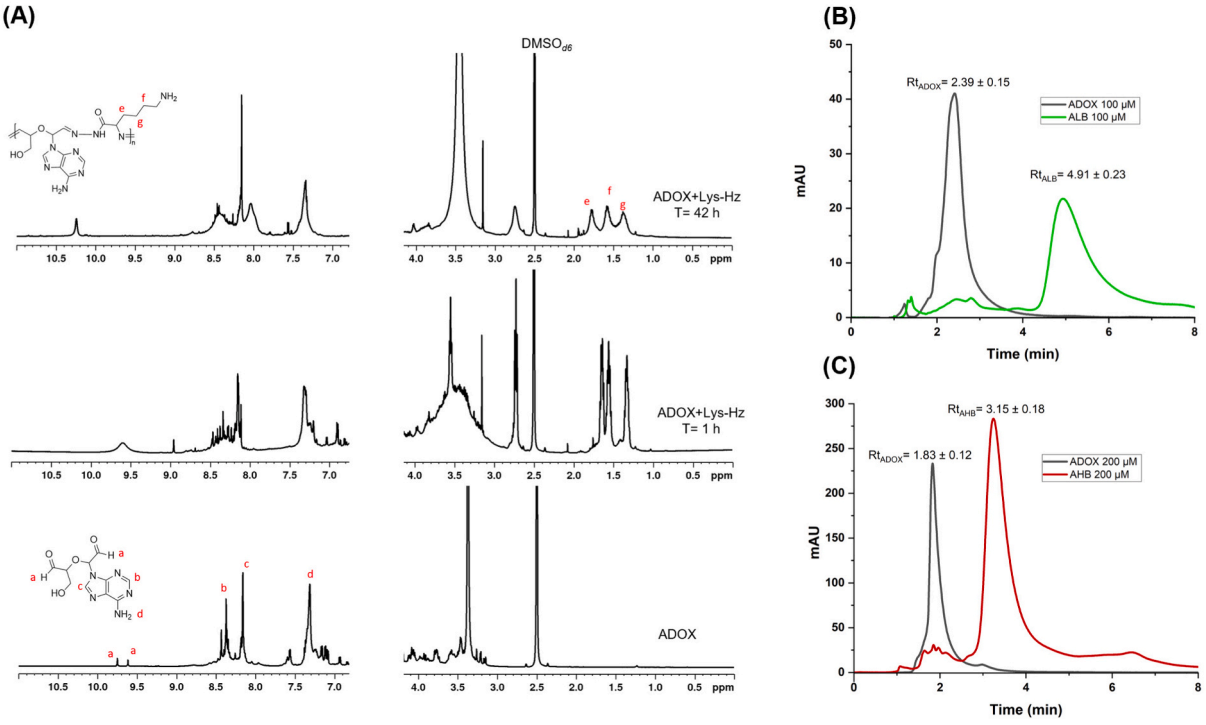

Fig. 2. Characterization of synthesized ADOX-biodynamers. (A) ^{1}HNMR spectra showing the time-dependent polymerization of ALB. HPLC analysis of the reaction mixtures of ADOX with (B) ALB (green) and (C) AHB (red) after 42 h for ALB hours, compared to free ADOX (black). (For interpretation of the references to colour in this figure legend, the reader is referred to the web version of this article.)

Based on these results, we concluded that the ADOX successfully reacted with each amino acid-Hz monomer, particularly Lys-Hz, His-Hz, and Phe-Hz, resulting in the formation of polymeric ADOX-biodynamers. The formed ADOX-biodynamer can offer a distinct advantage over conventional polymeric prodrugs in drug loading, as the drug (ADOX) is integrated in a 1:1 fashion with another monomer (amino acid-Hz) in the backbone. Many pH-responsive polymeric prodrugs that employ drug conjugation to polymer side chains suffer from low drug loading. This limitation is primarily due to poor conjugation efficiency caused by limited reaction efficiency and steric hindrance. Although a few studies have addressed such a challenge (*e.g.*, a pH-responsive PEG-doxorubicin conjugate achieved a conjugation efficiency of 38.1 % [47]), those still require an additional conjugation step to attach the drug to the polymer. In the case of ADOX-biodynamers, the polymer backbone itself is composed of the drug, and the drug is the substance that facilitates polymerization. Therefore, no additional conjugation steps are required after polymerization, eliminating the risk of limited conjugation efficiency. Additionally, since full drug activation involves restoring both terminal aldehyde groups, this system is expected to offer improved stability and safety.

3.2. pH-dependent ADOX release from ADOX-biodynamers

After confirming polymerization, we evaluated the stability of the ADOX-biodynamers at neutral pH and their acid-responsive drug release by monitoring ADOX release at pH 5.4, 6.4, and 7.4 using HPLC (Fig. S6, S7). In the case of ALB, the intensity of the ADOX peak increased over time at pH 5.4 with the cumulative release reaching approximately 38 % after 96 h. Meanwhile, less than 5 % of ADOX was released at pH 7.4. Similarly, ADOX release from AHB was significantly higher at pH 5.4, with approximately 22 % released after 96 h of incubation, compared to only 8 % at pH 7.4 (Fig. 3). Accordingly, both ADOX-biodynamers are expected to offer improved safety than the free drug under neutral conditions while selectively activating its efficacy under TME conditions. Among them, ALB showed greater potential for further studies owing to its higher stability at neutral pH and efficient pH-responsive drug release than AHB.

3.3. Safety profile of ADOX-biodynamer in physiological conditions

We next investigate the safety profile of ADOX-biodynamer (ALB) in comparison to free ADOX *in vitro*. The effect of ADOX and ALB on three cancer cell lines, HCT116, MCF-7, and SW480, was tested (Fig. 4A–C). The three cell lines were selected based on tumor types in which ADOX has been reported to be effective *in vivo* [17,18]. As a negative control, we used medium containing 0.4 % DMSO, which corresponds to the highest DMSO concentration present in samples containing either ADOX or ALB. This concentration was previously validated by MTT assay to have no significant cytotoxic effect on any of the tested cell lines (Fig. S8–S10), supporting its use in the experiments.

The results indicated that all tested cell lines exhibited high sensitivity to free ADOX. In HCT116, cell viability dropped below 10 % at 400 μM after 72 h of incubation (IC_{50}: 77.6 μM). However, when ADOX was delivered in its polymeric prodrug form, ALB, cell viability on this cell line increased to approximately 70 % under the same conditions (Fig. 4A). This trend was particularly pronounced in MCF-7 cells, where free ADOX (400 μM, 72 h) reduced cell viability to below 10 % (IC_{50}: 79.5 μM), whereas ALB had no significant effect (Fig. 4B). In SW480 cells, the most drug-sensitive line (IC_{50}: 29.2 μM), ALB treatment maintained cell viability above 60 % even at 200 μM, whereas free ADOX reduced viability to around 20 % under the same conditions (Fig. 4C).

The varying susceptibility of different cancer cell lines to ADOX can be attributed to intrinsic factors such as differences in drug uptake, efflux mechanisms, and DNA repair pathways [17]. Nevertheless, in all cell lines, treatment with the polymeric prodrug form, ALB, resulted in reduced toxicity, making it impossible to determine a reliable IC_{50} value under the tested conditions. This confirms the improved safety of the prodrug compared to ADOX, particularly in standard *in vitro* cell culture conditions at neutral pH.

In addition, we extended the evaluation of the cytotoxicity of ALB onto non-cancerous cells by testing on human bronchial epithelial 16HBE14o$^-$ cells. This cell line is immortalized with SV40 large T-antigen and is widely used to define chemotherapeutic regimens [48]. It is considered a non-cancerous cell line due to its physiological and phenotypic characteristics similar to native bronchial epithelial cells and is primarily used as a model for testing the toxicity of many drugs [42,49].

16HBE14o- cells were treated with ADOX and ALB at different concentrations for 72 h, and their viability was evaluated using MTT assay. The results (Fig. 5) showed that free ADOX exhibited significantly higher toxicity toward 16HBE14o$^-$ cells compared to the ALB at the same concentration under neutral conditions. At 100 μM, ALB demonstrated a significant improvement in cell viability, with over 70 % of cells remaining viable, while treatment with free ADOX reduced cell viability to below 20 %. This indicated a 5-fold increase in cell viability with ALB, highlighting its reduced toxicity in its inactive state. This confirms that the biodynamer design effectively minimizes off-target

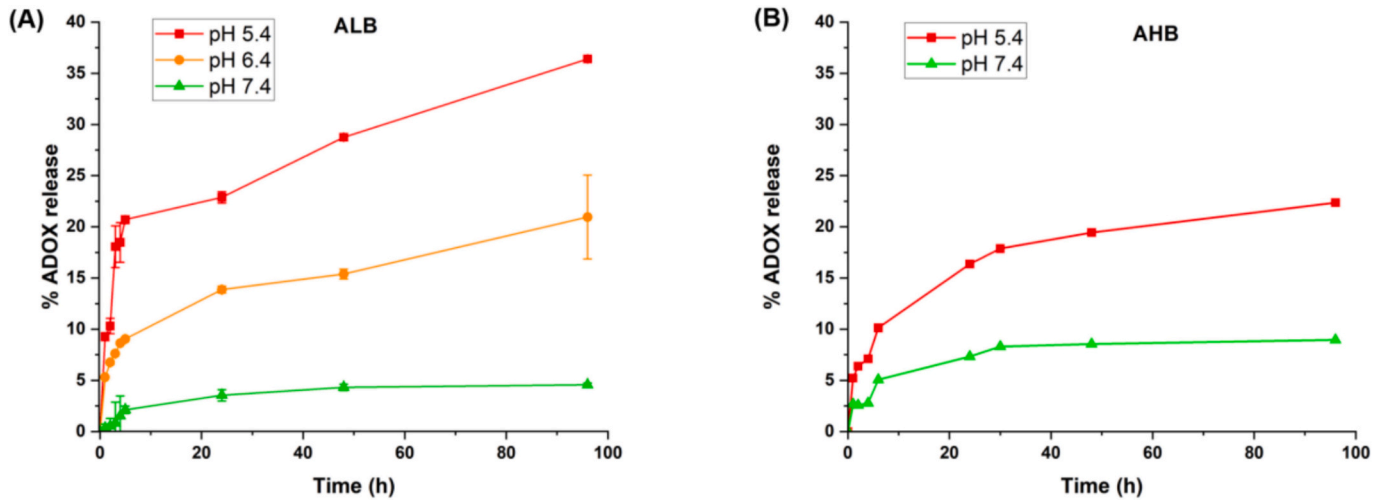

Fig. 3. Release profile of ADOX from ALB (A) and AHB (B) after 96 h incubation in 10 mM acetate buffer at pH 5.4, MES buffer at pH 6.4, and phosphate buffer at pH 7.4 ($n = 3$).

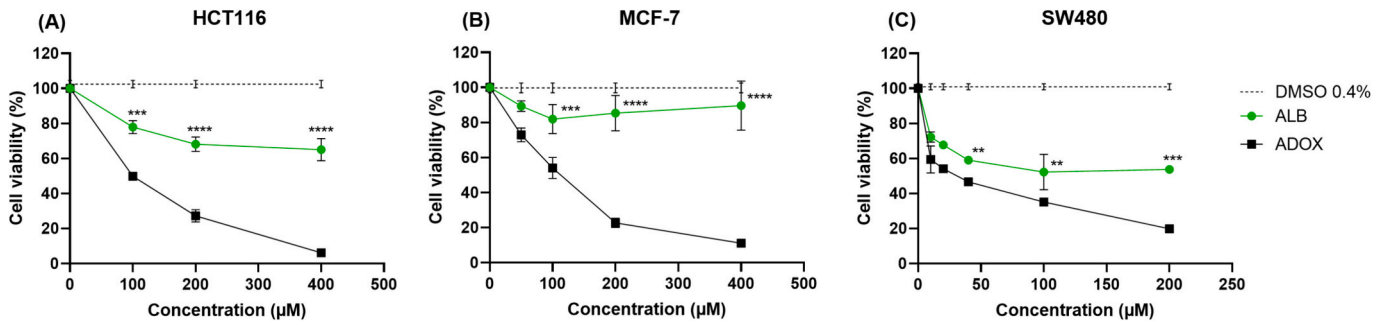

Fig. 4. Reduced effect of ALB compared to ADOX (0, 25, 50, 100, 200, and 400 μM) on the viability of cancer cell lines at neutral conditions: HCT116 (A), MCF-7 (B), and SW480 (C). Cell viability was analyzed using the MTT assay for 72 h, with a negative control of DMSO 0.4 %. Data are represented as the mean ± SD ($n = 5$, $N = 3$).

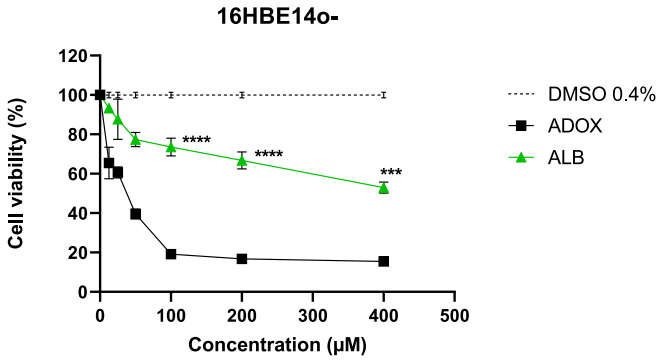

Fig. 5. Reduced effect of ALB compared to ADOX (0, 12.5, 25, 50, 100, 200, and 400 μM) on the viability of human bronchial epithelial 16HBE14o-. Cell viability was analyzed using the MTT assay for 72 h, with a negative control of DMSO 0.4 %. Data are represented as the mean ± SD (n = 5, N = 3).

toxicity in non-cancerous cells, supporting its potential for safer therapeutic applications.

3.4. pH-Dependent activity recovery of ADOX-biodynamer

The ADOX-biodynamer with improved safety should recover its anticancer activity under acidic conditions by releasing ADOX. Therefore, we examined the restoration of ALB activity under acidic conditions mimicking the pH of TME, using the same cell lines. Given the degradation rate of ALB under acidic conditions, it is optimal to expose it to a low-pH environment for at least 6 h, and preferably up to 4 days. However, prolonged incubation of cells in such acidic environments (pH 5.4–6.4) can affect their viability. To address this, we preactivated ALB under the pH of TME. Specifically, ALB was incubated in a 10 mM acetate buffer at pH 5.4 for 48 h to simulate its degradation and then treated on the cells for 72 h. The activity was assessed by MTT assay across all three cell lines and further evaluated by LDH assay in HCT116 cells.

Pre-activation of ALB under acidic conditions led to its degradation and subsequent release of ADOX. This significantly reduced the viability of all tested cell lines at 200 and 400 μM, compared to ALB without pre-activation, which represents its state under neutral conditions (Fig. 6A–C). In HCT116 cells, pre-activated ALB (active ALB) at 400 μM reached approximately 60 % of the anticancer activity observed with free ADOX at the same concentration.

The results of the LDH assay (Fig. 6D) further demonstrated the increased toxicity of active ALB on HCT116 cells compared to inactive ALB. Since LDH is an intracellular enzyme released upon cell membrane damage, its levels directly indicate cytotoxic effects. After incubating free ADOX with HCT116 cells for 72 h, over 70 % LDH release was observed, confirming its cytotoxicity to the cells. In contrast, ALB under neutral conditions exhibited a significantly lower LDH release of around 30 %, indicating reduced membrane damage and lower cytotoxicity of the polymeric prodrug. However, active ALB at acidic pH significantly increased LDH release up to 60 %, showing a modest difference compared to free ADOX at 400 μM. These results confirmed that the ALB activation induces cytotoxic effects and recovers the drug efficacy on HCT116 cells *via* the release of ADOX.

In the previous experiment, only ALB was pre-exposed to acidic conditions for an extended period to induce ADOX release prior to cell treatment, whereas free ADOX was applied without such pre-treatment. To allow a more accurate comparison, we additionally examined whether prolonged exposure of free ADOX to the same acidic conditions would affect its anticancer activity. The ADOX in the medium (100, 200, and 400 μM), without any pre-exposure, was compared with pre-exposed ADOX regarding their effects on cells.

The results indicated that the efficacy of free ADOX was significantly reduced under acidic conditions (Fig.S11), suggesting limited stability of ADOX in acidic environments. We hypothesize that the aldehyde group of ADOX becomes protonated under acidic conditions and undergoes oxidation during the pre-exposure process, resulting in a reduction in its effect on cells. Therefore, when ADOX is formed as a prodrug, like ALB, it can effectively circumvent this instability issue by protecting ADOX from protonation and oxidation, ensuring the direct release of ADOX in a low-pH environment.

Considering the previously observed ADOX release profile of ALB, the observed increased toxicity of ALB is reasonably attributed to the activity of the released ADOX, followed by its mechanism of action (MoA). It is well established that ADOX induces apoptosis through two primary mechanisms: by destabilizing the PIMT structure, thereby relieving its inhibitory effect on p53, and by enhancing both the expression and nuclear translocation of p53 [20]. We hypothesize that the ADOX-biodynamer shares a similar anticancer MoA with free ADOX. In apoptosis/necrosis staining experiments, both free ADOX and ALB induced significant levels of apoptosis in HCT116 cells (Fig. S12). This suggests that activated ALB exerts an apoptotic effect comparable to that of free ADOX. Nonetheless, the potential contribution of another building block of ALB, the Lys-Hz, to the biological activity and MoA of ALB cannot be entirely ruled out. For instance, studies have shown that lysine can suppress tumor growth and metastasis [49]. This suggests that incorporated amino acid monomers should be taken into account in future investigations aiming to elucidate the precise MoA of the ADOX-biodynamer.

3.5. Uptake study of ALB on cancer cells

In the previous experiment, the efficacy of ALB was evaluated after 72 h of incubation at an acidic pH. However, under physiological conditions, the possibility of ALB being taken up by cells before its

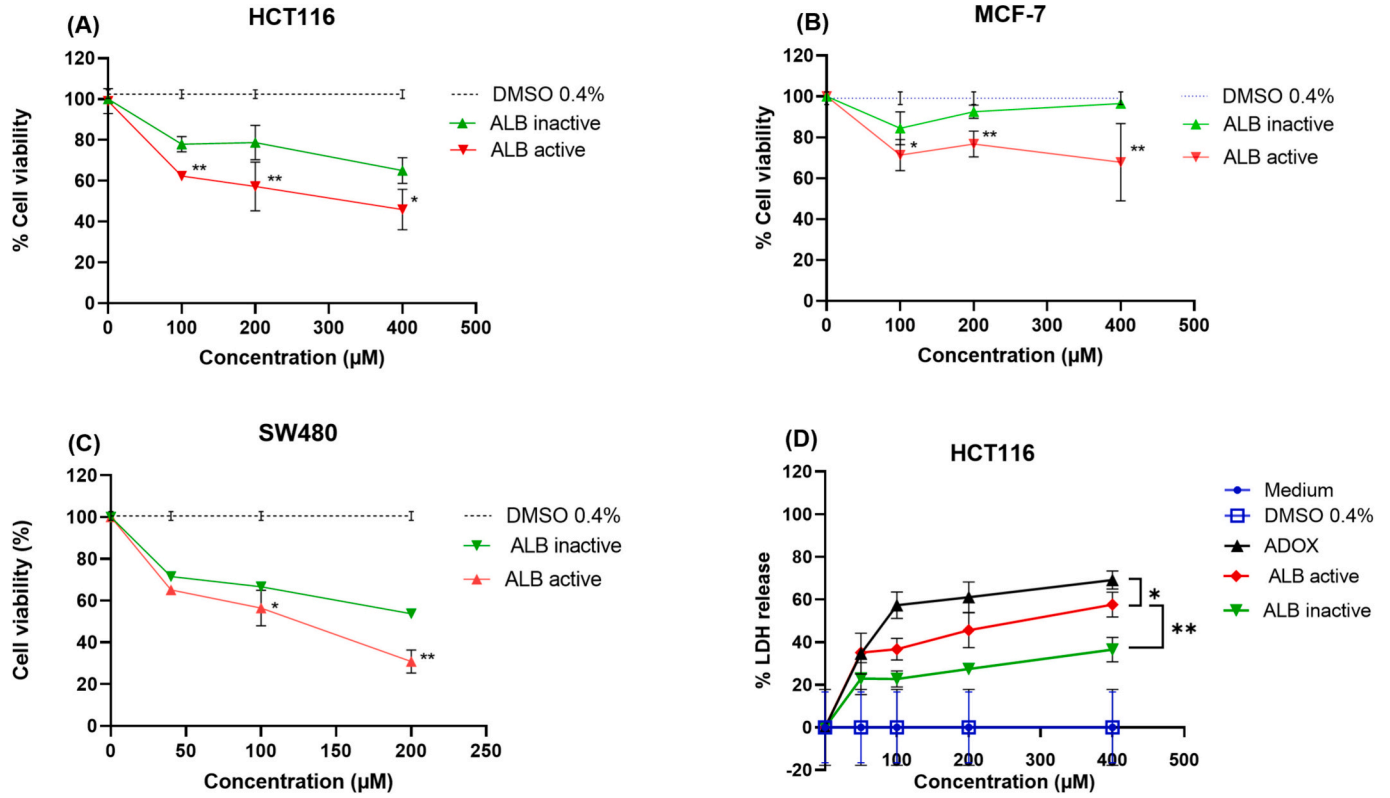

Fig. 6. Differential effect of inactive and active ALB on the viability of cancer cell lines: HCT116 (A), MCF-7 (B), and SW480 (C), and on LDH leakage from HCT116 cells for 72 h (D). Data are represented as the mean ± SD ($n = 5$, $N = 3$).

degradation in the TME cannot be overlooked. Therefore, the cell uptake rate under acidic conditions was assessed. ALB was labeled with Rhodamine and incubated with HCT116 cells in two different pH environments (pH 6.4 and pH 7.4) for 2 h. After the washing, HCT116 cells were stained and imaged by CLSM to visualize the cell uptake of ALB.

Resultingly, a significantly enhanced red signal, which represented Rho-ALB, was observed from the cells incubated at pH 6.4 compared to that at pH 7.4 (Fig. 7A). The z-stack image of the cells was further analyzed to validate their intracellular uptake and identify their localization within the cells. Consequently, the ALB is located not only on the membrane but also in the intracellular environment, particularly in the perinuclear region (Fig. 7B).

The SAHH, which is the target of ADOX, is primarily located in the cytoplasm and nucleus. Its cytoplasmic SAHH presence is crucial for regulating methylation reactions by maintaining low SAH levels, which otherwise inhibit methyltransferases. The nuclear localization of SAHH plays a role in epigenetic regulation by influencing DNA and histone methylation [50]. Therefore, ALB's ability to deliver ADOX to the nuclear region suggests that it may enhance its interaction with SAHH, yielding beneficial effects on tumor treatment.

Note that, even if the polymeric prodrug form, ALB, was taken up by the cells before releasing ADOX in the TME, it can still release ADOX inside the cells, particularly in compartments such as endosomes and lysosomes, where the lower pH values significantly enhance drug release. Similar mechanisms have been observed in other pH-responsive delivery systems; for instance, endogenous pH-sensitive nanoparticles of doxorubicin demonstrated efficient drug release under lysosomal conditions [51].

To further confirm the pH-dependent cellular uptake of ALB observed in Fig. 7A, we analyzed the cells using flow cytometry. Fig. 7C demonstrates a significantly higher uptake of ALB in cells at pH 6.4 relative to pH 7.4. Notably, the fluorescence intensity associated with internalized ALB at pH 6.4 was nearly twice as high as that at pH 7.4 (Fig. 7D). These findings aligned with the results indicated by CLSM, while providing a quantitative comparison.

Positively charged polymers are known to be taken up by cells more efficiently than negatively charged polymers [52–54]. For instance, guanidinium-functionalized poly (methacrylic acid) exhibited significantly higher internalization than unmodified poly (methacrylic acid). As the number of guanidinium groups increased, the polymer's negative charge decreased, leading to more efficient cellular uptake [53]. The superior internalization of cationic polymers is primarily driven by electrostatic interactions with the negatively charged cell membrane, which arises from the anionic head groups of phospholipids [55].

Similar to other cationic polymers, the enhanced cellular uptake of ALB may be attributed to its positive surface charge, which is modulated by the pH-responsive nature of the biodynamer. Indeed, zeta potential measurements revealed that ALB exhibits a higher positive charge at pH 6.4 (+25.98 mV) compared to pH 7.4 (+19.6 mV). This increase in surface charge is likely due to the partial degradation of the polymer backbone under acidic conditions, specifically the hydrolysis of imine and acylhydrazone linkages, which exposes free amine groups. The resulting increase in positive charge enhances electrostatic interactions with the negatively charged cell membrane, thereby facilitating more efficient cellular internalization of ALB, primarily *via* endocytosis. Additionally, the degradation of the polymer into shorter fragments at lower pH may further contribute to cellular uptake by promoting passive diffusion across the membrane. This pH-dependent uptake and toxicity profile highlights the potential of ALB for the selective delivery of ADOX to acidic tumor microenvironments, thereby reducing off-target effects on healthy tissues.

3.6. ADOX-biodynamer efficacy on tumor spheroids

Finally, we assessed the potential of ALB in a tumor spheroid model that more closely mimics the TME than a standard monolayer culture. As

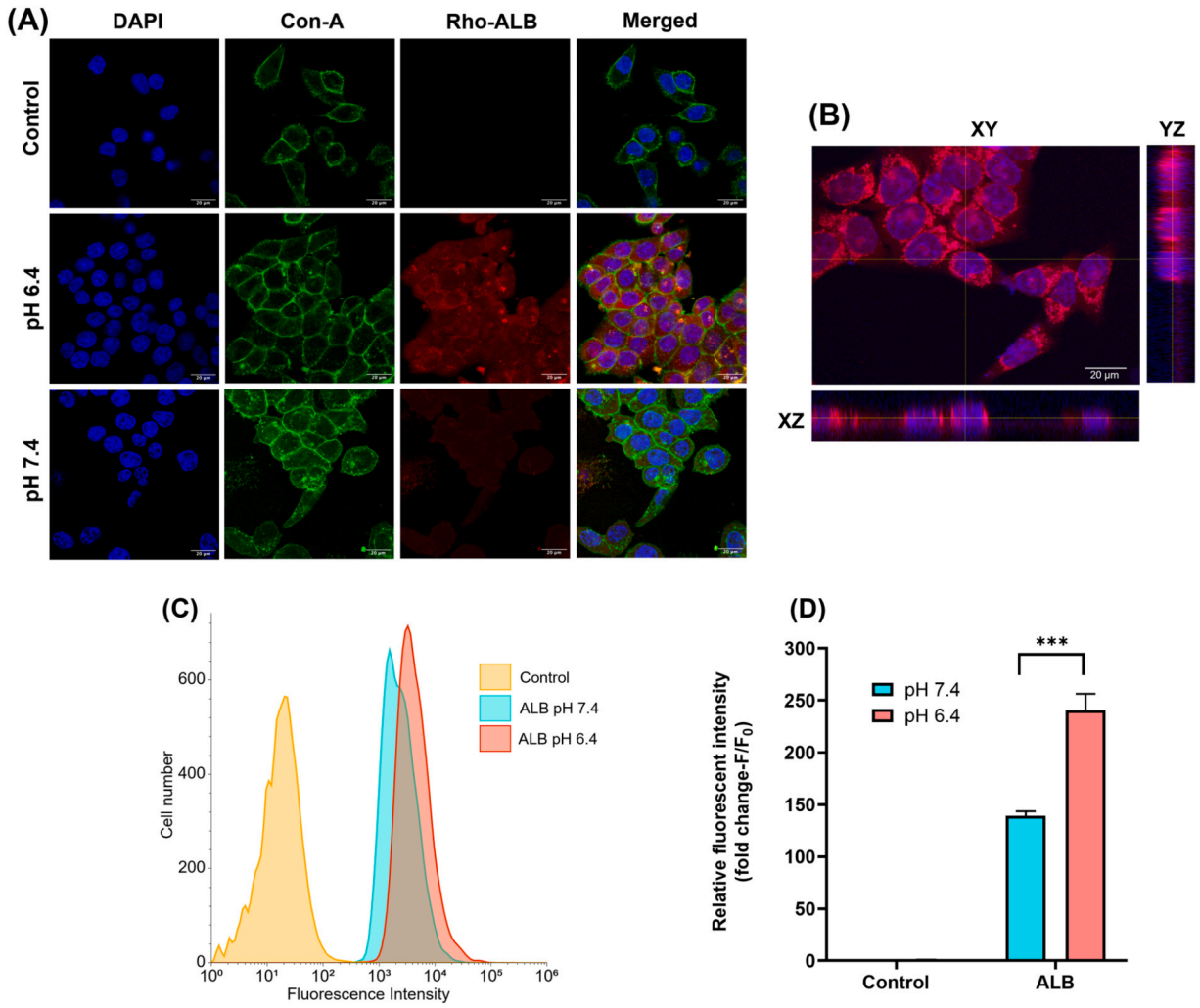

Fig. 7. (A) Uptake of ALB in HCT116 cells in different pH environments. The cells were incubated for 2 h with 60 μg/mL Rhodamine-labeled ALB in HBSS buffer adjusted to either pH 7.4 or 6.4. Cellular uptake was then visualized using CLSM. DAPI (blue) was used to stain nuclei, Con-A (green) marked the cell membranes, and Rhodamine (red) represented ALB. (B) Confocal microscopy z-stack imaging to localize the position of ALB within HCT116 cells after 2 h of incubation. (C) Histograms of ALB uptake by HCT116 cells at pH 6.4 and 7.4, measured by flow cytometry. (D) Comparison of the relative fluorescence intensity (expressed as fold change, with the fluorescence intensity of the control set as F_0) of the red signal between two ALB treatment conditions at pH 7.4 and 6.4 ($n = 3$). (For interpretation of the references to colour in this figure legend, the reader is referred to the web version of this article.)

discussed above, the monolayer cell culture has a limitation in mimicking the TME. Spheroids are well known for being able to more accurately mimic both main features found in solid tumors and the TME [56–58]. Similar to solid tumors, the spheroids comprised external layers with a high proliferation rate of cells. The high proliferation rate of cells in the spheroid periphery is due to their easier access to oxygen and nutrients [59,60]. In contrast, cells located in the interior of spheroids tend to be either senescent or necrotic due to a lack of oxygen (hypoxia) and nutrients [61]. Furthermore, in hypoxic environments, cancer cells convert pyruvate to lactate to obtain energy, a process known as the Warburg effect [62]. The accumulation of lactate in spheroids is responsible for the acidification of its interior (pH 6.5–7.2), which also occurs within *in vivo* solid tumors [59,60]. Thus, spheroids could serve as a higher-dimensional TME-mimicking model to test *in vitro* antiproliferative activity of ADOX-biodynamers.

For this purpose, we cultured HCT116 spheroids. Although ALB demonstrated higher safety and controlled activity in MCF-7 cells, spheroid formation with MCF-7 is more challenging than with HCT116 due to differences in cell–cell adhesion properties [63]. Additionally, the pH of the environment surrounding HCT116 spheroids is lower than that of MCF-7 spheroids due to higher glycolytic activity and lactate production [64]. This lower pH is more conducive to activating and evaluating the effects of our ADOX-biodynamers.

After 3 days of culture, HCT116 spheroids exhibit a compact and spherical shape, with a distinct outer core, and their diameter is approximately 500 ± 10 μm. Using a previously established method [65], the impact of ADOX and ALB on HCT116 spheroids was evaluated. Spheroids were imaged every 12 h over a period of 7 days to monitor changes in their morphology and size.

After 7 days of treatment, the results (shown in Fig. 8A) demonstrate the potent inhibitory effect of ALB on the growth of HCT116 spheroids across all testing concentrations (50, 100, 200, 400 μM) compared to non-treated spheroids (control). The higher the concentration of ALB treated with spheroids, the more significant the reduction of spheroid size. Remarkably, an approximate 40 % decrease in the spheroid area was observed after 7 days with 400 μM of ALB (Fig. 8B). The spheroids not only diminished in size but also exhibited signs of cell detachment, with dead cells peeling away from the outer layers, further evidenced by visualization in Fig. 8A. Untreated spheroids grew continuously, expanding in size throughout the 10-day culture period. The free ADOX-treated spheroid initially showed a decrease in size within 2 days, but subsequently, the spheroid's size began to increase.

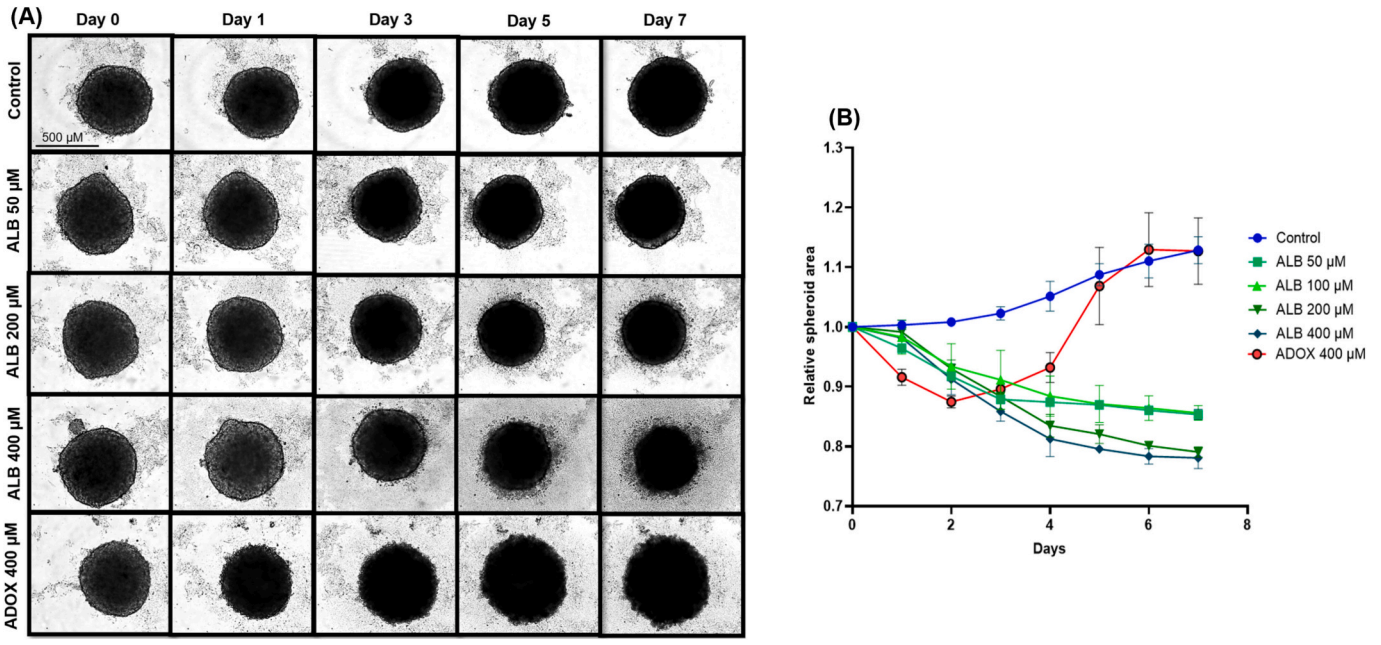

Fig. 8. (A) Images of spheroids were captured under a microscope at different time points after treatment with ALB and ADOX. Spheroids cultured in medium supplemented with 0.4 % DMSO served as the control. HCT116 spheroids were treated with ALB at concentrations (50, 100, 200, and 400 μM) and ADOX (400 μM). (B). The relative spheroid area of HCT116 spheroids was analyzed from the images of (A) ($n = 3$, $N = 3$).

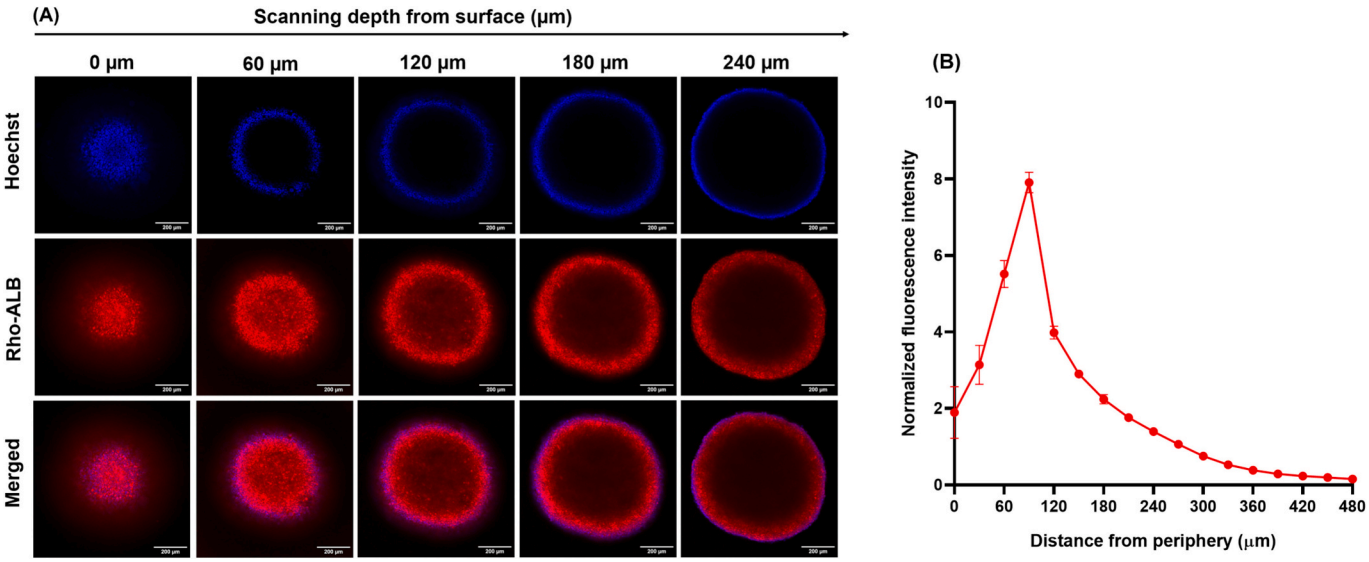

Fig. 9. (A) *Z*-stack images show the penetration of Rho-ALB in 3-day-old HCT116 spheroids. The spheroid was captured as a z-stack using 22 steps at 30 μm intervals. Analysis was performed on a z-projection of all the images representing a plane through the approximate center of the spheroid. (B) The rhodamine fluorescence intensity *versus* distance from the periphery of ALB in HCT116 spheroids. The normalized fluorescence intensity was calculated by the ratio of the fluorescence intensity to the area of the relevant slice ($n = 3$).

In addition, the impact of ALB was observed only after 2 days of treatment. Afterward, ALB continued to demonstrate effectiveness in inhibiting spheroid growth throughout the experimental time points. The hypothesis here is that the low pH environment within the spheroids facilitates the degradation of ALB during the 2 days when it penetrates them. This process leads to the accelerated release of ADOX within the spheroids, effectively inhibiting their growth.

To further investigate this phenomenon, the penetration capability of ALB within HCT116 spheroids was examined. The 3-day-old spheroids with a diameter of around 580 ± 20 μm were incubated with Rho-ALB (60 μg/mL) for 24 h, and the distribution and penetration depth of ALB were assessed by using CLSM with z-stack imaging. Representative confocal images from the periphery to the core of the spheroids (Fig. 9A), along with fluorescence intensity profiles (Fig. 9B) as a function of distance, are presented in Fig. 9.

The results demonstrated that the ALB polymer efficiently penetrates HCT116 spheroids, reaching depths of approximately 60–120 μm from the periphery, which suggests superior internalization and diffusion compared to reported chemotherapeutic agents. As widely reported in the literature, the deeper penetration of chemotherapeutic agents into the core of spheroids poses a significant challenge [66,67]. For instance, doxorubicin (10 μg/mL) typically penetrates only 20–60 μm into HCT116 spheroids after 24 h of incubation [67,68]. In larger spheroids with diameters greater than 500 μm, which we used in our study,

doxorubicin accumulation is primarily restricted to the outermost cell layers, with poor distribution toward the core. This limited penetration is attributed to multiple factors, including strong nuclear binding, tumor microenvironment acidity, and the action of efflux transporters such as P-glycoprotein (P-gp), which actively expel the drug from cells, reducing its retention in the spheroid core [69].

In contrast, due to its pH-responsive character, ALB may benefit from the acidic microenvironment within the HCT116 spheroid interior, facilitating the degradation of its polymeric backbone into smaller fragments and promoting the release of ADOX. This process may improve the diffusion and intra-tumoral penetration of ADOX, allowing it to reach deeper spheroid regions. The degree of penetration and its effect on inducing cell death in the spheroid need to be further investigated to understand the full impact of ADOX-biodynamers on the spheroids.

4. Conclusion

In this study, we proposed biodynamer-based polymeric prodrugs as a promising strategy to enhance the safety and restore the therapeutic efficacy of ADOX under the acidic conditions of the TME. The prodrugs were designed through the polymerization of ADOX and amino acid hydrazides *via* pH-responsive dynamic covalent bonds. This design enables accelerated drug release in the acidic TME while also offering advantages over conventional polymer–drug conjugates, including higher drug incorporation, improved safety, and enhanced structural stability.

In vitro experiments demonstrated that ADOX-biodynamers showed significantly reduced cytotoxicity under neutral conditions compared to free ADOX across all tested cell lines. Notably, in the presence of ALB, the viability of non-cancerous cells increased by approximately 5-fold relative to free ADOX, which is attributed to the inactive form of ALB at neutral pH that prevents premature drug release and minimizes off-target toxicity. In contrast, under acidic conditions mimicking the TME, ADOX release from ALB was accelerated by approximately 8-fold, leading to a recovery of up to 60 % of the anticancer efficacy of ADOX in cancer cells. Moreover, positively charged ADOX-biodynamers, such as ALB, exhibited nearly 2-fold increased cellular uptake in acidic environments. After internalization, ALB was predominantly localized in the cytoplasm and near the nucleus, where its molecular target, SAHH, is highly expressed. These findings suggest that ALB can serve as an effective carrier for delivering ADOX to tumor cells.

These observations were further validated using an *in vitro* tumor tissue model (HCT116 spheroids), which better mimics the *in vivo* TME. In this model, restored ADOX activity was confirmed by significant reductions in spheroid size, increased cell detachment, and efficient intratumoral penetration.

Taken together, ADOX-biodynamers present a new approach to overcoming the limitations of free ADOX by facilitating its selective delivery, protecting it from premature degradation, and enabling pH-triggered reactivation at the tumor site. These promising results support the application of ADOX-biodynamers in animal models, including investigations of *in vivo* efficacy, biodistribution, and renal clearance. Continued research on structural and formulation optimization for improved solubility, along with deeper investigation into the MoA, will further substantiate their therapeutic potential. Ultimately, this dynamic covalent chemistry-based polymeric prodrug strategy provides a compelling platform for addressing the safety and selectivity challenges of conventional chemotherapeutics and may contribute to the development of next-generation targeted cancer therapies.

CRediT authorship contribution statement

Thi Thu Nguyen: Writing – original draft, Visualization, Validation, Methodology, Investigation, Formal analysis, Data curation. **Jan Hemmer:** Writing – review & editing, Methodology, Investigation, Formal analysis. **Alexandra K. Kiemer:** Writing – review & editing, Supervision, Resources, Methodology. **Britta Diesel:** Writing – review & editing, Validation, Supervision, Methodology, Investigation, Formal analysis, Data curation. **Sangeun Lee:** Writing – review & editing, Supervision, Project administration, Methodology, Investigation, Funding acquisition, Data curation, Conceptualization.

Declaration of generative AI and AI-assisted technologies in the writing process

During the preparation of this manuscript, we used Grammarly and ChatGPT to improve the language and readability. After using these tools, we reviewed and edited the content as needed and took full responsibility for the content of the publication.

Acknowledgements

The authors deeply acknowledge Marijas Juris's technical support in the CLSM experiments and Prof. Marc Schneider from the Department of Pharmacy, Biopharmaceutics and Pharmaceutical Technology at Saarland University for their support in instrument availability and engagement in discussions.

Thi Thu Nguyen acknowledges financial support from the Saarland Graduate Funding Programme (GraduSaar), Saarland, Germany.

Appendix A. Supplementary data

Supplementary data to this article can be found online at https://doi.org/10.1016/j.jconrel.2025.114538.

Data availability

Data will be made available on request.

References

[1] U. Anand, et al., Cancer chemotherapy and beyond: current status, drug candidates, associated risks and progress in targeted therapeutics, Genes Dis. 10 (4) (2023), https://doi.org/10.1016/j.gendis.2022.02.007.
[2] M. Pourmadadi, et al., Recent advancements in the targeted delivery of gemcitabine: harnessing nanomedicine for enhanced cancer therapy, OpenNano 13 (13) (2023 Sep), https://doi.org/10.1016/j.onano.2023.100177.
[3] A. Bisht, D. Avinash, K.K. Sahu, P. Patel, G. Das Gupta, B. Das Kurmi, A Comprehensive Review on Doxorubicin: Mechanisms, Toxicity, Clinical Trials, Combination Therapies and Nanoformulations in Breast Cancer, Springer, 2025 Jan 01, https://doi.org/10.1007/s13346-024-01648-0.
[4] B.M. Ejeta, M.K. Das, S. Das, Recent advances in paclitaxel drug delivery: challenges, innovations, and future directions, J. Angiother. 8 (8) (2024 Aug) 1–12, https://doi.org/10.25163/angiotherapy.889867.
[5] S. Man, Y. Lu, L. Yin, X. Cheng, L. Ma, Potential and Promising Anticancer Drugs from Adenosine and its Analogs, Elsevier Ltd., 2021 Jun 01, https://doi.org/10.1016/j.drudis.2021.02.020.
[6] M. Kamle, et al., Camptothecin and its Derivatives: Advancements, Mechanisms and Clinical Potential in Cancer Therapy, Springer, 2024 Nov 01, https://doi.org/10.1007/s12032-024-02527-x.
[7] I. Khurram, et al., Thapsigargin and its Prodrug Derivatives: Exploring Novel Approaches for Targeted Cancer Therapy through Calcium Signaling Disruption, Springer, 2025 Jan 01, https://doi.org/10.1007/s12032-024-02541-z.
[8] F. Li, T. Jiang, Q. Li, X. Ling, Camptothecin (CPT) and its derivatives are known to target topoisomerase I (Top1) as their mechanism of action: did we miss something in CPT analogue molecular targets for treating human disease such as cancer? Am. J. Cancer Res. 7 (12) (2017) 2350–2394.
[9] D. Mahalingam, et al., A phase II, multicenter, single-arm study of mipsagargin (G-202) as a second-line therapy following sorafenib for adult patients with progressive advanced hepatocellular carcinoma, Cancers (Basel) 11 (6) (2019), https://doi.org/10.3390/cancers11060833.
[10] B.L. Mirkin, R.F. O'dea, H.P. Hogenkamp, Cytotoxic Action of Adenosine Nucleoside and Dialdehyde Analogues on Murine Neuroblastoma in Tissue Culture: Structure-Activity Relationships1 [Online]. Available, http://aacrjournals.org/cancerres/article-pdf/47/14/3650/2427799/cr0470143650.pdf, 1987.
[11] V. Ramakrishnan, R.T. Borchardt, Adenosine dialdehyde and neplanocin a: potent inhibitors of S-adenosylhomocysteine hydrolase in neuroblastoma N2a cells, Neurochem. Int. 10 (4) (1987), https://doi.org/10.1016/0197-0186(87)90068-4.
[12] B.A. Johnson, J. Najbauer, D.W. Aswad, Accumulation of substrates for protein L-isoaspartyl methyltransferase in adenosine dialdehyde-treated PC12 cells, J. Biol.

Chem. 268 (9) (1993 Mar) 6174–6181, https://doi.org/10.1016/S0021-9258(18)53235-X.
[13] U. Patel-Thombre, R.T. Borchardt, Adenine nucleoside dialdehydes: potent inhibitors of bovine liver S-adenosylhomocysteine hydrolase, Biochemistry 24 (5) (1985), https://doi.org/10.1021/bi00326a010.
[14] Y. Huang, S. Wang, X. Ding, et al., Inhibition of S-adenosyl-L-homocysteine hydrolase alleviates alloimmune response by down-regulating CD4+ T-cell activation in a mouse heart transplantation model, Ann. Transl. Med. 8 (23) (2020 Dec) 1582, https://doi.org/10.21037/atm-20-2899.
[15] M. Shiota, A. Takeuchi, A. Yokomizo, E. Kashiwagi, K. Tatsugami, S. Naito, Methyltransferase inhibitor adenosine dialdehyde suppresses androgen receptor expression and prostate cancer growth, J. Urol. 188 (1) (2012), https://doi.org/10.1016/j.juro.2012.02.2553.
[16] J.H. Kim, et al., Adenosine dialdehyde suppresses MMP-9-mediated invasion of cancer cells by blocking the Ras/Raf-1/ERK/AP-1 signaling pathway, Biochem. Pharmacol. 86 (9) (2013 Nov) 1285–1300, https://doi.org/10.1016/J.BCP.2013.08.022.
[17] R. Ghemrawi, et al., DNA and protein methyltransferases inhibition by adenosine dialdehyde reduces the proliferation and migration of breast and lung cancer cells by downregulating autophagy, PLoS One 18 (7) (2023 Jul), https://doi.org/10.1371/journal.pone.0288791.
[18] T. Chatterjee, et al., Adenosine dialdehyde, a methyltransferase inhibitor, induces colorectal cancer cells apoptosis by regulating PIMT:p53 interaction, Biochem. Biophys. Res. Commun. 684 (2023 Dec), https://doi.org/10.1016/j.bbrc.2023.149134.
[19] A. Dasgupta, K.J. Jung, S.J. Jeong, J.N. Brady, Document details - inhibition of methyltransferases results in induction of G_2/M checkpoint and programmed cell death in human T-lymphotropic virus type 1-transformed cells, J. Virol. 82 (1) (2008 Jan) 49–59.
[20] C. Schwerk, K. Schulze-Osthoff, Methyltransferase inhibition induces p53-dependent apoptosis and a novel form of cell death, Oncogene 24 (47) (2005) 7002–7011, https://doi.org/10.1038/sj.onc.1208855.
[21] P.K. Chiang, Biological effects of inhibitors of S-adenosylhomocysteine hydrolase, Pharmacol. Ther. 77 (2) (1998) 115–134.
[22] J.P. Neenan, S.M. Opitz, C.L. Cooke, M.A. Ussery, T.C. Morrill, L.M. Eckel, Adenosine dialdehyde analogs I: regioselective synthesis of adenosine monoaldehydes, Bioorg. Med. Chem. Lett. 6 (12) (1996) 1381–1386, https://doi.org/10.1016/0960-894X(96)00234-X.
[23] B. Bostrom, H.P.C. Hogenkamp, B.L. Mirkin, Inhibitory effect of adenosine dialdehyde on in situ murine neuroblastoma growth, Cancer Res. 48 (21) (1988).
[24] X. Wang, et al., Smart drug delivery systems for precise cancer therapy, Acta Pharm. Sin. B 12 (11) (2022), https://doi.org/10.1016/j.apsb.2022.08.013.
[25] J. Du, L.A. Lane, S. Nie, Stimuli-responsive nanoparticles for targeting the tumor microenvironment, J. Control. Release 219 (2015), https://doi.org/10.1016/j.jconrel.2015.08.050.
[26] R. Yang, et al., Tumor microenvironment responsive metal nanoparticles in cancer immunotherapy, Front. Immunol. 14 (2023), https://doi.org/10.3389/fimmu.2023.1237361.
[27] M. Alsehli, Polymeric nanocarriers as stimuli-responsive systems for targeted tumor (cancer) therapy: recent advances in drug delivery, Saudi Pharm. J. 28 (3) (2020), https://doi.org/10.1016/j.jsps.2020.01.004.
[28] P.D. Ramírez-García, et al., A pH-responsive nanoparticle targets the neurokinin 1 receptor in endosomes to prevent chronic pain, Nat. Nanotechnol. 14 (12) (2019), https://doi.org/10.1038/s41565-019-0568-x.
[29] M.H. Cho, E.S. Choi, S. Kim, S.H. Goh, Y. Choi, Redox-responsive manganese dioxide nanoparticles for enhanced MR imaging and radiotherapy of lung cancer, Front. Chem. 5 (DEC) (2017), https://doi.org/10.3389/fchem.2017.00109.
[30] Q. Hu, P.S. Katti, Z. Gu, Enzyme-responsive nanomaterials for controlled drug delivery, Nanoscale 6 (21) (2014), https://doi.org/10.1039/c4nr04249b.
[31] S. Chu, X. Shi, Y. Tian, F. Gao, pH-responsive polymer nanomaterials for tumor therapy, Front. Oncol. 12 (2022), https://doi.org/10.3389/fonc.2022.855019.
[32] V. Estrella, et al., Acidity generated by the tumor microenvironment drives local invasion, Cancer Res. 73 (5) (2013), https://doi.org/10.1158/0008-5472.CAN-12-2796.
[33] Z. Kooshan, L. Cárdenas-Piedra, J. Clements, J. Batra, Glycolysis, the sweet appetite of the tumor microenvironment, Cancer Lett. 600 (2024) 217156, https://doi.org/10.1016/j.canlet.2024.217156.
[34] L. Zeroug-Metz, S. Lee, Biodynamers: applications of dynamic covalent chemistry in single-chain polymer nanoparticles, Drug Deliv. Transl. Res. 14 (12) (2024) 3599–3607, https://doi.org/10.1007/s13346-024-01665-z.
[35] Y. Liu, J.M. Lehn, A.K.H. Hirsch, Molecular biodynamers: dynamic covalent analogues of biopolymers, Acc. Chem. Res. 50 (2) (2017), https://doi.org/10.1021/acs.accounts.6b00594.
[36] A. Nguyen, R. Böttger, S.D. Li, Recent trends in bioresponsive linker technologies of prodrug-based self-assembling nanomaterials, Biomaterials 275 (2021), https://doi.org/10.1016/j.biomaterials.2021.120955.
[37] S. Lee, et al., PH-dependent morphology and optical properties of lysine-derived molecular biodynamers, Mater. Chem. Front. 4 (3) (2020), https://doi.org/10.1039/c9qm00651f.
[38] Y. Liu, et al., pH-responsive dynaplexes as potent apoptosis inductors by intracellular delivery of Survivin siRNA, Biomacromolecules 24 (8) (2023), https://doi.org/10.1021/acs.biomac.3c00424.
[39] S. Lee, et al., Proteoid biodynamers for safe mRNA transfection via pH-responsive nanorods enabling endosomal escape, J. Control. Release 353 (2023), https://doi.org/10.1016/j.jconrel.2022.12.018.
[40] M.A.M. Kamal, J. Bassil, B. Loretz, A.K.H. Hirsch, S. Lee, C.-M. Lehr, Arg-biodynamers as antibiotic potentiators through interacting with gram-negative outer membrane lipopolysaccharides, Eur. J. Pharm. Biopharm. 200 (2024) 114336, https://doi.org/10.1016/j.ejpb.2024.114336.
[41] L. Zeroug-Metz, et al., Fluorescent histidine-derived biodynamers as biocompatible and highly water-soluble copper(ii)-sensors, RSC Appl. Polym. 2 (6) (2024 Sep) 1124–1138, https://doi.org/10.1039/d4lp00126e.
[42] B. Diesel, N. Ripoche, R.T. Risch, S. Tierling, J. Walter, A.K. Kiemer, Inflammation-induced up-regulation of TLR2 expression in human endothelial cells is independent of differential methylation in the TLR2 promoter CpG island, Innate Immun. 18 (1) (2012 Feb) 112–123, https://doi.org/10.1177/1753425910394888.
[43] S. Gao, L. Li, I. Vohra, D. Zha, L. You, Differential metal-binding properties of dynamic acylhydrazone polymers and their sensing applications, R. Soc. Open Sci. 4 (8) (2017), https://doi.org/10.1098/rsos.170466.
[44] S.I. Stoyanov, A.A. Dobrev, L.M. Antonov, Structure investigations of N-acylated imines by means of UV-vis spectroscopy, Mon. Chem. - Chem. Mon. 125 (3) (1994), https://doi.org/10.1007/BF00811311.
[45] Y. Liu, M.C.A. Stuart, E. Buhler, J.M. Lehn, A.K.H. Hirsch, Proteoid Dynamers with tunable properties, Adv. Funct. Mater. 26 (34) (2016), https://doi.org/10.1002/adfm.201601612.
[46] I. Kaya, F. Kolcu, G. Demiral, H. Ergül, E. Kiliç, Synthesis and characterization of imine polymers of aromatic aldehydes with 4-amino-2-methylquinoline via oxidative polycondensation, Des. Monomers Polym. 18 (1) (2015), https://doi.org/10.1080/15685551.2014.971395.
[47] J. Song, et al., Schiff-linked PEGylated doxorubicin prodrug forming pH-responsive nanoparticles with high drug loading and effective anticancer therapy, Front. Oncol. 11 (2021), https://doi.org/10.3389/fonc.2021.656717.
[48] A.L. Cozens, et al., CFfR expression and chloride secretion in polarized immortal human bronchial epithelial cells, Am. J. Respir. Cell Mol. BioI. 10 (1994) 38–47.
[49] J. Montroy, et al., The safety and efficacy of lysine analogues in cancer patients: a systematic review and meta-analysis, Transfus. Med. Rev. 31 (3) (2017) 141–148, https://doi.org/10.1016/j.tmrv.2017.03.002.
[50] D. Kloor, et al., Expression and localization of S-adenosylhomocysteine-hydrolase in the rat kidney following carbon monoxide induced hypoxia, Cell. Physiol. Biochem. 19 (1–4) (2007), https://doi.org/10.1159/000099192.
[51] W. Wu, et al., Endogenous pH-responsive nanoparticles with programmable size changes for targeted tumor therapy and imaging applications, Theranostics 8 (11) (2018), https://doi.org/10.7150/thno.23459.
[52] L. Chen, J.D. Simpson, A.V. Fuchs, B.E. Rolfe, K.J. Thurecht, Effects of surface charge of hyperbranched polymers on cytotoxicity, dynamic cellular uptake and localization, hemotoxicity, and pharmacokinetics in mice, Mol. Pharm. 14 (12) (2017), https://doi.org/10.1021/acs.molpharmaceut.7b00611.
[53] Y.Y. Khine, M. Callari, H. Lu, M.H. Stenzel, Direct correlation between zeta potential and cellular uptake of poly(methacrylic acid) post-modified with guanidinium functionalities, Macromol. Chem. Phys. 217 (20) (2016), https://doi.org/10.1002/macp.201600161.
[54] Y.K. Oh, D. Suh, J.M. Kim, H.G. Choi, K. Shin, J.J. Ko, Polyethylenimine-mediated cellular uptake, nucleus trafficking and expression of cytokine plasmid DNA, Gene Ther. 9 (23) (2002), https://doi.org/10.1038/sj.gt.3301735.
[55] B. Sharma, C. Peetla, I.M. Adjei, V. Labhasetwar, Selective biophysical interactions of surface modified nanoparticles with cancer cell lipids improve tumor targeting and gene therapy, Cancer Lett. 334 (2) (2013), https://doi.org/10.1016/j.canlet.2013.03.011.
[56] M. Zimmermann, C. Box, S.A. Eccles, Two-dimensional vs. three-dimensional in vitro tumor migration and invasion assays, Methods Mol. Biol. 986 (2013) 227–252, https://doi.org/10.1007/978-1-62703-311-4_15.
[57] E. Fennema, N. Rivron, J. Rouwkema, C. van Blitterswijk, J. De Boer, Spheroid culture as a tool for creating 3D complex tissues, Trends Biotechnol. 31 (2) (2013 Feb) 108–115, https://doi.org/10.1016/J.TIBTECH.2012.12.003.
[58] S. Breslin, L. O'Driscoll, Three-dimensional cell culture: the missing link in drug discovery, Drug Discov. Today 18 (5–6) (2013 Mar) 240–249, https://doi.org/10.1016/J.DRUDIS.2012.10.003.
[59] G. Mehta, A.Y. Hsiao, M. Ingram, G.D. Luker, S. Takayama, Opportunities and challenges for use of tumor spheroids as models to test drug delivery and efficacy, J. Control. Release 164 (2) (2012 Dec) 192–204, https://doi.org/10.1016/J.JCONREL.2012.04.045.
[60] O. Trédan, C.M. Galmarini, K. Patel, I.F. Tannock, Drug resistance and the solid tumor microenvironment, J. Natl. Cancer Inst. 99 (19) (2007 Oct) 1441–1454, https://doi.org/10.1093/jnci/djm135.
[61] A.I. Minchinton, I.F. Tannock, Drug penetration in solid tumours, Nat. Rev. Cancer 6 (2006) 583–592, https://doi.org/10.1038/nrc1893.
[62] W.H. Koppenol, P.L. Bounds, C.V. Dang, Otto Warburg's contributions to current concepts of cancer metabolism, Nat. Rev. Cancer 11 (5) (2011 May) 325–337, https://doi.org/10.1038/nrc3038.
[63] S.J. Han, S. Kwon, K.S. Kim, Challenges of applying multicellular tumor spheroids in preclinical phase, Cancer Cell Int. 21 (1) (2021), https://doi.org/10.1186/s12935-021-01853-8.
[64] A.P. Andersen, M. Flinck, E.K. Oernbo, N.B. Pedersen, B.M. Viuff, S.F. Pedersen, Roles of acid-extruding ion transporters in regulation of breast cancer cell growth in a 3-dimensional microenvironment, Mol. Cancer 15 (1) (2016), https://doi.org/10.1186/s12943-016-0528-0.
[65] C. Dahlem, et al., First small-molecule inhibitors targeting the RNA-binding protein IGF2BP2/IMP2 for cancer therapy, ACS Chem. Biol. 17 (2) (2022 Feb) 361–375, https://doi.org/10.1021/acschembio.1c00833.

[66] I.F. Tannock, C.M. Lee, J.K. Tunggal, D.S. Cowan, M.J. Egorin, Limited penetration of anticancer drugs through tumor tissue: a potential cause of resistance of solid tumors to chemotherapy, Clin. Cancer Res. 8 (3) (2002) 878–884.
[67] A. Tchoryk, et al., Penetration and uptake of nanoparticles in 3D tumor spheroids, Bioconjug. Chem. 30 (5) (2019), https://doi.org/10.1021/acs.bioconjchem.9b00136.
[68] L.Q. Thao, et al., Doxorubicin-bound albumin nanoparticles containing a TRAIL protein for targeted treatment of colon cancer, Pharm. Res. 33 (3) (2016), https://doi.org/10.1007/s11095-015-1814-z.
[69] H.R. Mellor, R. Callaghan, Accumulation and distribution of doxorubicin in tumour spheroids: the influence of acidity and expression of P-glycoprotein, Cancer Chemother. Pharmacol. 68 (5) (2011), https://doi.org/10.1007/s00280-011-1598-8.